Nano Research 2014, 7(9): 1280–1290
DOI 10.1007/s12274-014-0492-1
Research Article
ISSN 1998-0124
CN 11-5974/O4

Nitrogen-doped graphene supported Pd@PdO core–shell clusters for C–C coupling reactions

Baojiang Jiang[1], Sanzhao Song[1], Jianqiang Wang[2], Ying Xie[1], Wenyi Chu[1], Hongfeng Li[1], Hui Xu[1], Chungui Tian[1], and Honggang Fu[1] (✉)

[1] *Key Laboratory of Functional Inorganic Material Chemistry, Ministry of Education of the People's Republic of China, Heilongjiang University, Harbin 150080, China*
[2] *Shanghai Synchrotron Radiation Facility (SSRF), Shanghai Institute of Applied Physics, Chinese Academy of Sciences, Shanghai, China*

Received: 22 February 2014
Revised: 3 May 2014
Accepted: 4 May 2014

KEYWORDS
graphene,
nitrogen-doped,
Pd cluster,
catalyst,
Suzuki reaction

ABSTRACT

The introduction of nitrogen significantly decreases the metal particle size and improves the performance of metal-based graphene-supported catalysts. In this work, the density functional theory is used to understand the interaction between nitrogen-doped graphene and Pd@PdO clusters. Experiments show that small size Pd@PdO clusters (1–2 nm) can be grown uniformly on nitrogen-doped graphene sheets by a facile oxidation–reduction method. The nanoscale interaction relationship between nitrogen-doped graphene and Pd@PdO clusters is investigated through X-ray photoelectron spectroscopy (XPS) and X-ray absorption spectra (XAS). The composite catalysts are applied in Suzuki–Miyaura reactions giving high yields and good structural stability. These results have potential impact in design and optimization of future high performance catalyst materials for cross coupling reactions.

1 Introduction

Pd-catalyzed cross coupling reactions are one of the most important methods for C–C bond formation in organic chemistry [1–4]. Their outstanding importance has been demonstrated by the Nobel Prize in Chemistry 2010. However, to realize the practical application of Pd catalysts in C–C cross coupling reactions such as the Suzuki–Miyaura reaction, several important improvements still await to be made, e.g., reduction of the Pd particle size, increase of the catalyst stability, and a decrease of the amount of Pd used [5, 6]. The use of Pd clusters, the sizes of which range from sub-nanometer to about 2 nm, could greatly improve the catalytic properties because of their unique electrical structure, large surface area, and high proportion of surface atoms [7, 8]. Moreover, PdO clusters can also be used as a highly efficient heterogeneous catalyst for Suzuki coupling reactions [9]. However, the surface energy increases with decreasing particle size, which usually leads to serious aggregation of Pd clusters [10]. Moreover, the morphology and size of Pd clusters

Address correspondence to fuhg@vip.sina.com

may be changed during the Suzuki–Miyaura reaction, which will decrease the catalytic performance. To avoid these problems, the introduction of support materials could effectively stabilize the Pd clusters and enhance the catalytic properties. In addition, compared to monometallic nanoparticles, core–shell type structures such as Pd@PdO could exhibit improved electronic, physiochemical, and catalytic properties by virtue of the complex electronic interactions between the core and the shell component [11].

Recently, many studies have suggested that carbon-based support materials can be doped with heteroatoms such as nitrogen and boron to create strong, beneficial catalyst–carbon support interactions which substantially enhance catalyst activity and stability due to the small particle size and the narrower size distribution of catalyst [12]. For example, a density functional theory (DFT) study suggested that in nitrogen-doped Vulcan carbon the nitrogen atoms significantly enhance the Pd adsorption on the surface [13]. Graphene is a novel one atom-thick two-dimensional graphitic carbon material, which has attracted increasing interest due to its high surface area and good chemical stability [14–18], and can also be used as an ideal support material for growing and anchoring noble metal Pd clusters for the Suzuki–Miyaura reaction [19]. In particular, N-doped graphene (NDG) has an increased conductivity as the nitrogen atoms contribute additional electron density in the parent matrix, which will also influence the metal–NDG interaction behavior [20]. The nitrogen in graphene also plays a significant role in determining the nucleation rate and growth process of Pd clusters. However, the direct observation of the spatial relationship between the Pd catalyst and the NDG support is still lacking and, in particular, further understanding of the interaction between the nitrogen and metal Pd particles is needed.

This study uses DFT to calculate the binding energy between NDG and Pd@PdO clusters. Then we prepared Pd@PdO clusters supported on NDG in order to further investigate the effect of nitrogen on the growth of Pd@PdO clusters. Pd nanoparticles supported on reduced graphene oxide generally exhibit large size (>5 nm) and poor distribution (5–20 nm). In our synthesis process, high quality and smooth graphene sheets were obtained from expanded graphite by a quenching method. This smooth support material is beneficial for the uniform distribution of small size metal clusters. Moreover, the N element in NDG can not only stabilize the embedded Pd@PdO clusters, but also promote the catalytic activity for Suzuki–Miyaura reaction.

2 Experimental

2.1 Synthesis of Pd@PdO–N doped graphene (Pd@PdO–NDG)

All chemical reagents were obtained from commercial sources and used without further purification. The graphite powder was bought from Qingdao Tianyuan Company. H_2SO_4 (98%), HNO_3 (65%), $KMnO_4$, H_2O_2, HCl, ammonia, ethanol, and methanol were obtained from Beijing Chemical Co., Ltd. The ethylene glycol, palladium acetate, and polyvinylpyrrolidone (PVP) were obtained from Sigma-Aldrich Trading Co., Ltd.

In a typical experimental procedure, briefly, we prepared the expanded graphite (EG) using the H_2SO_4, HNO_3, and $KMnO_4$ as the oxidant and intercalation agent. Then, the single- and few-layer graphene was obtained from EG by quenching method, which is similar to our previous work [17]. For purifying the graphene, we selected the simple density gradient separation method to remove the un-exfoliated EG [21]. The density gradient solution contains ethanol and ethylene glycol with different ratios. After the separation process, the graphene sheets were dried, and dispersed in ammonia for a subsequent hydrothermal process to obtain NDG sheets similar to our previous work [22].

Finally, the Pd@PdO–NDG was produced by a simple reduction reaction of palladium acetate as follows: 150 mL of a methanol solution including 0.05 g of NDG and 2.5 g of PVP was sonicated for 15 min to produce a homogeneous solution. Then, the solution was transferred to a three necked flask for the subsequent reflux procedure. Meanwhile, 20 mL of a methanol solution of palladium acetate (0.22 mmol of $Pd(C_2H_3O_2)_2$) was added into the above solution with continuous stirring and refluxing at 65 °C for 2 h similar to a previous report [23]. After the reduction

reaction, the black samples (Pd@PdO–NDG) were separated by high-speed centrifugation, washed several times with ethanol and distilled water, and dried at below than 60 ℃. For comparison, the Pd@PdO–graphene was obtained by a similar method as follows: The graphene sheets were also prepared from the expanded graphite by the quenching method. Then, 150 mL of a methanol solution including 0.05 g of graphene and 2.5 g of PVP was sonicated for 15 min to produce a homogeneous solution. 20 mL of a methanol solution of palladium acetate (0.22 mmol) was added into above solution with continuous stirring and refluxing for 2 h at 65 ℃ in a three necked flask. Finally, the Pd@PdO–graphene was obtained after centrifugation, washing, and drying.

2.2 Catalytic experiments

The Suzuki cross coupling reaction procedure: A flask was charged with phenylboronic acid (0.75 mmol), K_2CO_3 (1.25 mmol), an ethanol solution of Pd@PdO–NDG (4 mL, catalyst 5 mg·mL^{-1}), ethanol (4 mL), and different substrates (0.5 mmol). The flask was sealed and stirred in a preheated oil bath (80 ℃) for 1 h. After cooling to room temperature, the mixture was filtered, followed by removing a 10 μL aliquot of the mixture for high-performance liquid chromatography (HPLC) analysis. Purification of mixture was completed using petroleum ether and ethyl acetate as the eluent in a small column of silica gel. Then, the final pure products were obtained by evaporating the solvent. All the isolated products were analyzed by ^{1}H nuclear magnetic resonance (NMR) spectroscopy. In the recycling tests of the catalyst for Suzuki–Miyaura reaction, five consecutive cycles were tested. After each cycle, the mixture was diluted with ethanol and shaken. The entire mixture was filtered and washed thoroughly with ethanol and water to ensure the removal of all the products from the catalyst surface. The same amount of dry catalyst and then fresh phenylboronic acid and different substrate solutions were added to the catalytic system for the next run.

2.3 Density functional theory calculations

Calculations were performed within the DFT framework embedded in the DMol^3 code. The exchange-correlation energy was treated with the Perdew–Wang functional of the general gradient approximation (GGA) form. A DND basis set (double-numerical plus d-DNP basis), which is comparable to Gaussian 6-31G* basis sets, was used in the calculations. For the core treatment, all electrons were explicitly included. Moreover, to avoid spurious interactions between the periodic images along the z axis, a vacuum region with a length of 15 Å was used. The stable configure-ations were obtained by geometry optimization from the ideal unrelaxed structures. The whole optimization procedure was repeated until the forces on the atoms were less than 0.002 Ha·Å^{-1} and the energy change less than 1.0×10^{-5} Ha·atom^{-1}.

2.4 Characterization

The powder X-ray diffraction (XRD) patterns of the as-prepared products were recorded using a Rigaku D/max-IIIB diffractometer with Cu Kα radiation. The morphology and structure of as-prepared products were observed by high-resolution transmission electron microscopy (HRTEM, JEM-2100) with an acceleration voltage of 200 kV. X-ray photoelectron spectroscopy (XPS) was performed on a VG ESCALAB MK II with a Mg Kα (1253.6 eV) achromatic X-ray source. Thermogravimetric analysis was performed on a TG (TA, Q600) thermal analyzer in air with a heating rate of 10 K·min^{-1}. The metal Pd ion concentration was measured by inductively coupled plasma–atomic emission spectroscopy (ICP–AES) (Optima-7000DV).

The X-ray absorption data at the Pd K-edge of the samples were recorded at room temperature in transmission mode using ion chambers or in the fluorescence mode with silicon drift fluorescence detector at beam line BL14W1 of the Shanghai Synchrotron Radiation Facility (SSRF), China. The station was operated with a Si (311) double crystal monochromator. During the measurements, the synchrotron was operated at energy of 3.5 GeV and a current in the range 150–210 mA. The photon energy was calibrated with the first inflection point of Pd K-edge in Pd metal foil. Data processing was performed using the program ATHENA. All fits to the EXAFS data were performed using the program ARTEMIS.

3 Results and discussion

Theoretical investigations concerning the adsorption energy, nature of binding, and charge transfer were performed to confirm the effect of N doping on the interfacial interactions and the stabilities of the systems. DFT calculations were employed to evaluate the binding strength between Pd or PdO clusters and NDG. To facilitate a comparison, the adsorption energy between Pd or PdO clusters and a graphene sheet was also considered. The numerical results are listed in Table S1 (in the Electronic Supplementary Material (ESM)). The adsorption energies, arising from physisorption between Pd or PdO clusters and graphene are about –2.21 and –2.29 eV, respectively.

However, when the PdO clusters approach NDG, the adsorption energy of the system decreases significantly (–3.61 eV), suggesting the existence of strong covalent chemical adsorption between them. Similar results are also found for the Pd–NDG system. Figures 1(a) and 1(b) show the density of states (DOS) for Pd@PdO–NDG and Pd@PdO–graphene systems, respectively. The black line in Fig. 1(a) represents the total density of states (TDOS) of each element before the Pd@PdO clusters come into contact with NDG, while the red line indicates the TDOS of each element after contacting with NDG. The calculation results indicate the TDOS of Pd, which are mainly composed of Pd 4d states [24], shift to a lower energy position. Moreover, the TDOS for C atoms and N atoms are also changed significantly. In contrast, when Pd@PdO clusters are adsorbed on graphene, the TDOS of each element is nearly unchanged, as shown in Fig. 1(b). Therefore, it can be expected that the interaction between Pd@PdO and NDG is much stronger than that between Pd@PdO and graphene, and N doping enhances the surface chemisorption of Pd on the graphene sheet. Furthermore, the strong Pd–graphene support interactions will control the Pd nanoparticle size and dispersion, since the nature of support will

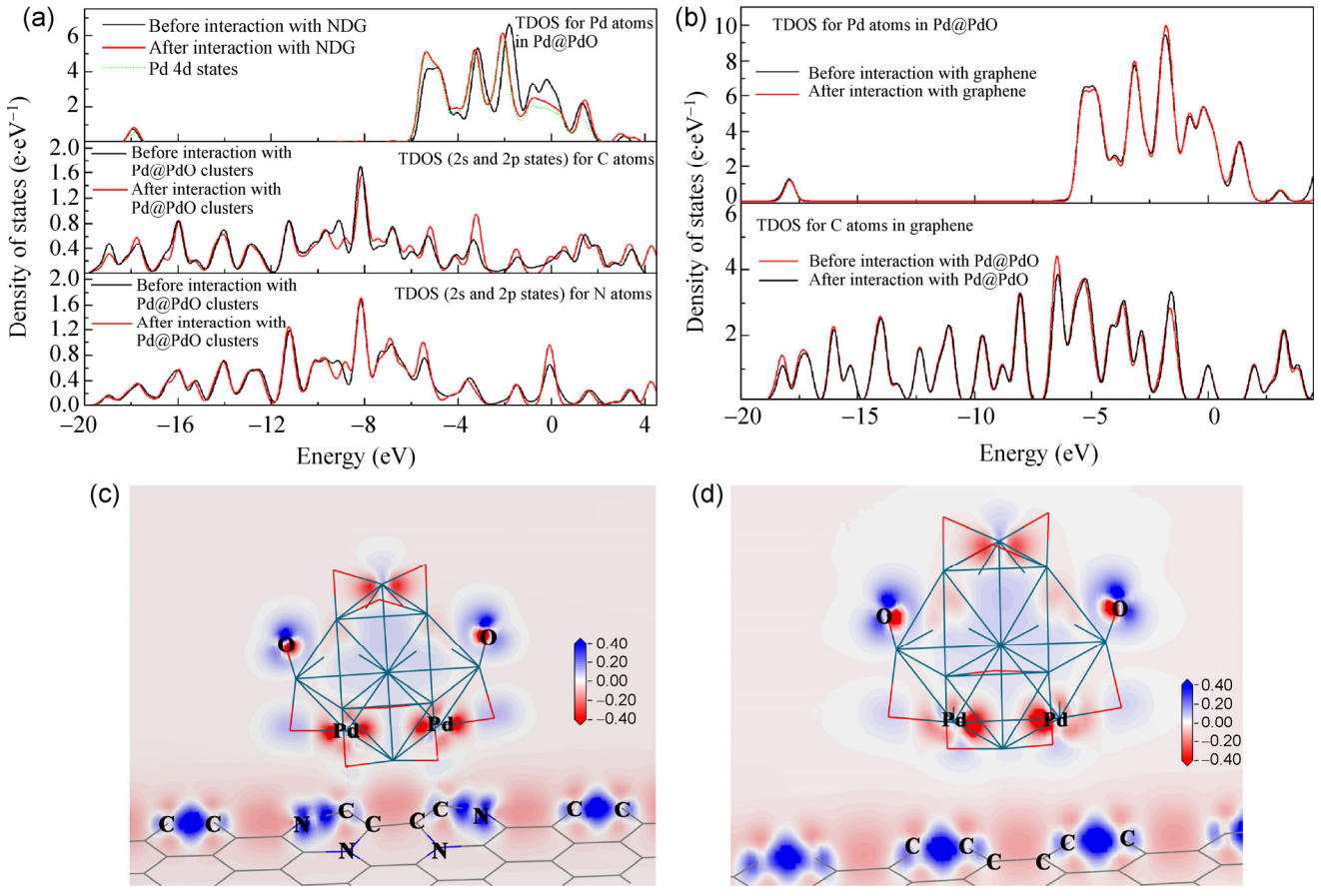

Figure 1 DOS for Pd@PdO–NDG (a) and Pd@PdO– raphene (b); Electron-density difference diagrams for Pd@PdO–NDG (c) and Pd@PdO–grapheme (d).

govern the nucleation and growth processes during deposition of metal particles.

Figures 1(c) and 1(d) depict the electron density differences (EDD) diagrams for Pd@PdO–NDG and Pd@PdO–graphene, respectively. The positive (in blue) or negative (in red) regions indicate where the electron density is enriched or depleted. For the Pd@PdO–NDG (Fig. 1(c)) system, the electron density around N atoms is enhanced, while that around C atoms in N–C bonds is weakened, as compared to the Pd@PdO–graphene shown in Fig. 1(d). Meanwhile, the Mulliken population for Pd in isolated Pd@PdO cluster is about 0.46, and the corresponding values for N and C in the isolated NDG are calculated to be –0.30 and 0.12 respectively. After Pd@PdO cluster comes into contact with NDG, the Mulliken population of the Pd in Pd@PdO cluster is changed from 0.46 to 0.86, and those of N and C atoms are changed to –0.27 and 0.03, which means there is considerable electron transfer between Pd and NDG. The electron transfer process possibly implies the formation of chemical bonds between Pd@PdO and NDG in Pd@PdO–NDG system. However, when Pd@PdO clusters adsorb on graphene (Fig. 1(d)), the change in Mulliken population of the C atoms in contact varies slightly from 0.00 to –0.05, and that of the Pd atoms still remain positive (0.46). Therefore, the dopant nitrogen atoms serve as a mediator to activate nearby carbon atoms, leading to the enhancement of Pd adsorption. Furthermore, due to the large electron affinity of nitrogen, the nucleation and the growth of Pd@PdO clusters on NDG surface will also be influenced, which will result in small-sized, well-dispersed, high-stability Pd@PdO clusters being anchored on graphene.

Subsequently, Pd@PdO clusters anchored NDG for use as composite catalysts were obtained by a facile synthesis method to complement the theoretical investigation. The detailed morphology and structure of the as-prepared composite catalyst were characterized using transmission electron microscopy (TEM), and the results are exhibited in Fig. 2. Figure 2(a) shows that graphene within the composite is an ultrathin sheet with few folds and crinkles, indicating that graphene obtained from expanded graphite has a more stable and flat structure than that graphene obtained from graphite oxide. It is interesting to note that these very small clusters are well distributed on the graphene sheets. From the measured particle size distributions, shown in the inset in Fig. 2(a), the average particle size is about 1.8 nm ± 0.6 nm. Moreover, the HRTEM images (left inset in Fig. 2(b)) show the interplanar spacing of the particle lattice is 0.226 nm, which agrees well with the (111) lattice spacing of face centered cubic Pd [25]. Interestingly, the Pd clusters (< 1.5 nm in diameter) exhibit an irregular external structure which is marked by the white arrows, possibly due to the partial surface oxidation of the Pd clusters to forming PdO (right inset in Fig. 2(b)). In order to identify the role of N doping, Pd–graphene samples were also prepared (Fig. S1 in the ESM). It is clearly observed that many larger Pd nanoparticles (> 10 nm) are loaded on the graphene, indicating that nitrogen doping in graphene can efficiently control the nucleation rate and growth process of Pd clusters. The DFT studies in Fig. 1 have shown that C–N defects and N interstitials in carbon substrates can serve as local heterogeneous Pd nucleation sites. Moreover, it can be stated that Pd nucleation preferentially occurs on regions of defective carbon as opposed to well ordered graphitic carbon. The structures of Pd@PdO–NDG were further characterized by XRD. The XRD patterns are shown as Fig. S2 in the ESM, and the peaks located at 2θ = 26.4, 54.5, and 77.4° are attributed to the (002), (004), and (110) diffraction facets of NDG, respectively. The peak at 39.4° in Fig. S2 corresponds to the (111) facets of palladium crystal [26]. However, a weak peak at 42.2° could also be observed, which is possibly from the (111) facets of PdO. These results suggest that the Pd@PdO–NDG composite catalysts have successfully been produced. Additionally, the Pd content in Pd@PdO–NDG was investigated by thermogravimetric analysis (TG-DSC) in air (Fig. S3 in the ESM). On the basis of the TG measurements, it is estimated that the Pd loading in Pd@PdO–NDG is about 14 wt.%, which is close to the ICP–AES analysis result for Pd content (15.5 wt.%).

XPS can be used to analyze the surface layer element composition, chemical state, and electronic structure of solid catalyst materials. Thus, XPS was used to further study the electronic structure change and the nitrogen doping effect (Fig. 3). The Pd–graphene was also studied as a reference. Figure 3(a) shows the

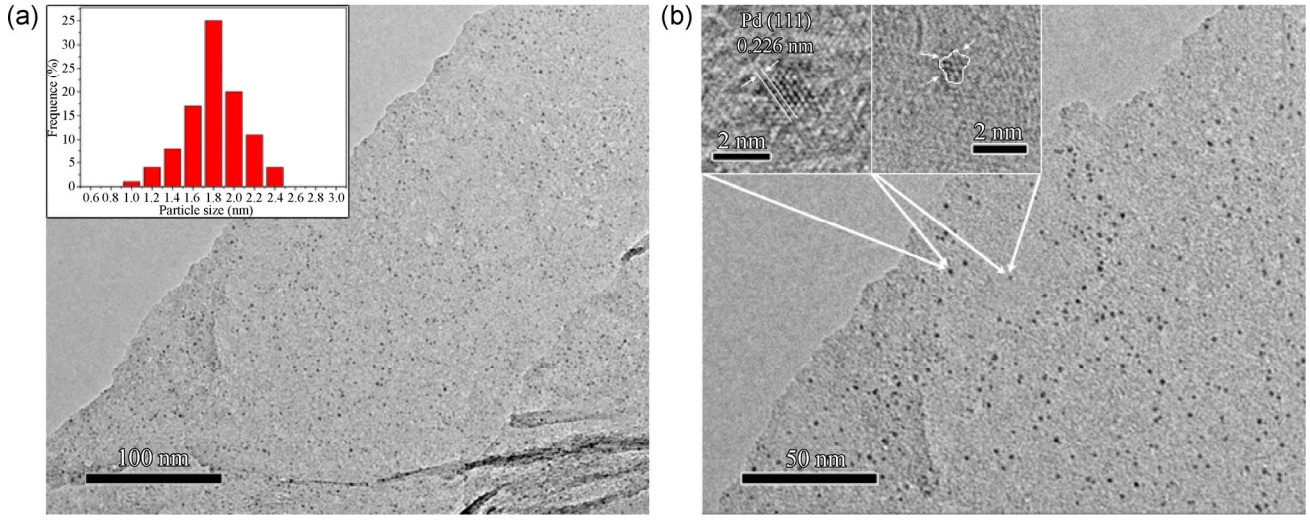

Figure 2 TEM images of the Pd@PdO–NDG catalyst; the particle size distribution and the HRTEM images of Pd@PdO clusters are shown as insets in (a) and (b), respectively.

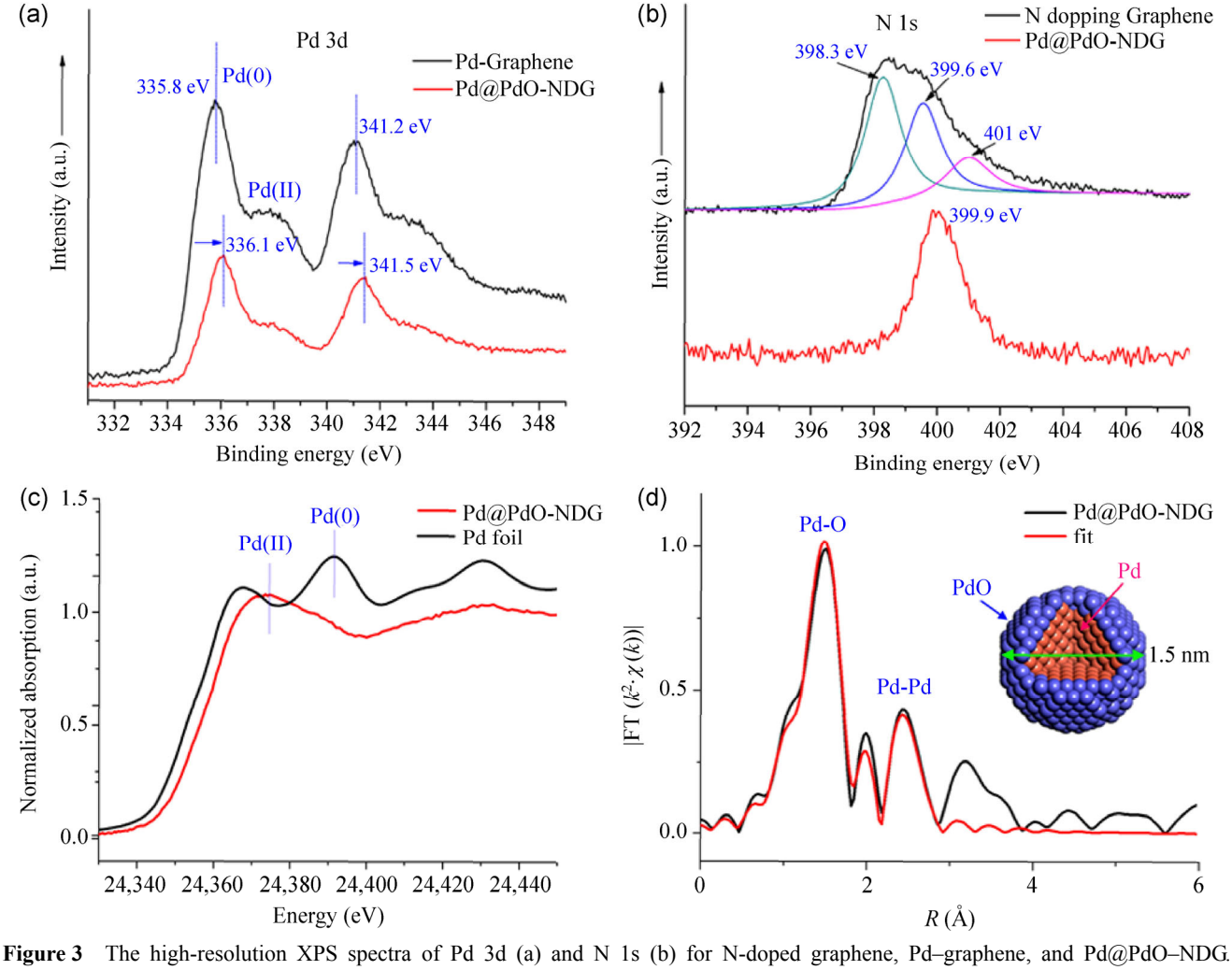

Figure 3 The high-resolution XPS spectra of Pd 3d (a) and N 1s (b) for N-doped graphene, Pd–graphene, and Pd@PdO–NDG. Comparison of the Pd K-edge XANES spectra for Pd@PdO–NDG and Pd foil (c). Fourier transform of k^2-weighted EXAFS data for the same sample of Pd@PdO–NDG (d) and the inset is a structure schematic of the Pd@PdO clusters.

high-resolution Pd 3d spectra. For Pd–graphene, the two peaks located at 335.8 and 341.2 eV can be assigned to Pd $3d_{3/2}$ and Pd $3d_{5/2}$ of metallic Pd(0), respectively [27]. The shoulder peaks at 337.8 and 343.2 eV are which are consistent with the reported values for Pd(II), confirming the presence of PdO species on the surface of Pd. Interestingly, for Pd@PdO–NDG, Pd peaks obviously shift toward higher binding energy compared to those of Pd–graphene. Normally, this kind of shift is induced by a change in electronic structure or coordination environment [16, 28], which can be attributed to the presence of strong interactions between Pd@PdO and NDG, and the effect of the small size of Pd@PdO clusters. In the Pd@PdO–NDG system, the nitrogen atoms have more electrons and change the electron density around carbon atoms, leading to the enhanced adsorption energy of Pd on graphene sheets (based on the DFT results), which is beneficial to the growth of Pd@PdO clusters on the graphene sheet. In addition, according to the XPS measurements, the nitrogen concentration is about 4.0 atom%. Furthermore, three different types of nitrogen in NDG, namely pyridinic nitrogen (398.3 eV), pyrrolic nitrogen (399.6 eV), and sp^3 C–N bonded nitrogen (401 eV) can be seen in Fig. 3(b). However, for Pd@PdO–NDG, the pyrrolic nitrogen (399.9 eV) is the main component [29]. The pyrrolic nitrogen atoms donate π-electron density to the carbon network of the graphene lattice and contribute to the sp^2 character of the graphene network. Therefore, we believe the metal Pd@PdO interacts with the pyrrolic nitrogen to form a stable chemisorbed structure. Moreover, the pyrrolic nitrogen peak is also shifted toward high energy after the adsorption process, which further proves the strong interaction between NDG and Pd@PdO.

To support the above analysis, X-ray absorption spectra (XAS) measurements were also performed, since these are sensitive to the valence and local structures of investigated elements [16, 30]. Figure 3(c) displays the Pd K-edge of the X-ray absorption near edge structure spectra (XANES) for Pd@PdO–NDG together with a reference spectrum of Pd foil. For the Pd foil reference, the absorption threshold resonance, appearing between 24,360 and 24,380 eV corresponds to the electronic transitions that arise from the 1s state to the unoccupied 4p states above Fermi level [31]. The second (24,385 eV) and third (24,435 eV) peaks correspond to 1s→dp and 1s→dsp transitions, respectively. The absorption threshold resonance position and intensity are sensitive to changes in electron occupancy in the valence orbital and ligand field environments of the absorber. However, the Pd K-edge for Pd@PdO–NDG shows a distinct shift toward higher energy relative to the reference spectrum of Pd foil, which is in accord with the XPS results. This kind of shift is normally induced by a change of metal's electronic structure. This shows the presence of strong interface interaction and electron transfer between Pd@PdO and NDG. Furthermore, the spectrum of Pd@PdO–NDG also exhibits a small feature at 24,372 eV, indicating the presence of Pd(II). In contrast, the intensity of the metallic Pd peak at 24,370 eV decreases significantly, indicating the oxidation of Pd clusters in the Pd@PdO, which is also in agreement with the XPS results. The Fourier transform of the k^2-weighted EXAFS data for Pd@PdO–NDG is exhibited in Fig. 3(d) along with reference data for bulk metallic Pd. The results show the first-shell Pd–O signal and the Pd–Pd signal, indicating that the Pd(II) ion was formed directly on the surface of Pd clusters, in good agreement with the XANES and XPS results. The structural parameters derived from the Pd K-edge EXAFS data analyses are shown in Table S2 in the ESM. The Pd–Pd coordination number in Pd foil is found to be 9.7 ± 0.5. However, for Pd@PdO–NDG, the coordination number is decreased to 2.1 ± 0.2, reflecting a decrease in the average coordination number, as expected in the case of small sized Pd clusters. The coordination number derived from XAS is a nonlinear function of particle diameter, and it has been widely used in EXAFS analysis to determine the size of the nanoparticles. Therefore, based on the Pd crystal cell parameters and our physical model, the particle diameter of Pd@PdO clusters is about 1.5 nm with an approximate surface single layer PdO structure (Table S2), which is very close to the HRTEM results. A schematic of the structure of Pd@PdO is also shown as an inset in Fig. 3(d). Furthermore, the detailed structure schematics for Pd@PdO–NDG and Pd@PdO–graphene are shown as Scheme S1 in the ESM. It is therefore believed that

the introduction of nitrogen into the graphene support network can also potentially increase the utilization of the noble-phase metal through improvements in dispersion, catalytic activity, and durability.

The practical application of Pd@PdO–NDG catalysts in C–C cross coupling reactions such as Suzuki–Miyaura reaction were tested using phenylboronic acid and different substrates in the presence of stabilized Pd@PdO–NDG catalysts. Table 1 gives the reaction conditions and results for the different substrates. As shown in Table 1, both reactions can be successfully performed, providing complete conversions of 100% and high yields of 96% of the corresponding Suzuki reactions products after 1 h at 80 ˚C, respectively. Entry no. 3 shows a slightly lower yield, but is still higher than that obtained with other Pd catalysts in the same time in previous reports, which can be attributed to the small size of the Pd@PdO clusters with a high ratio of surface atoms [32]. In contrast, Pd@PdO–graphene—which has relatively large and aggregated nanoparticles—exhibits low yields for the Suzuki–Miyaura reaction (the detailed results are shown in Table S3 in the ESM). Therefore N-dopant induced alteration of the catalyst electronic structure clearly influences the catalytic reaction. For example, one study showed that C–N surface species interactions with a decorating Pt nanoparticle phase result in a shift to higher binding energy which may reduce the detrimental strong adsorption of intermediates on the Pt surface, resulting in enhancement of catalysis [33]. The purified products for the Suzuki reaction were analyzed by ^{1}H NMR, and the results are listed in the ESM. The Suzuki coupling reaction involves an oxidation-addition reaction, the transfer of negative ions to the metal Pd(II) center, and a reduction-elimination reaction [34]. During the reaction, the formation of chemical bonds between the metal Pd and the support material could enhance the structural stability of metal Pd@PdO resulting in enhanced catalytic performance. In general, dopant nitrogen atoms could serve as a mediator to activate nearby carbon atoms, leading to the enhancement of Pd adsorption. Therefore, large numbers of small-sized, well-dispersed Pd@PdO clusters are obtained which have more catalytic active centers for the coupling reaction. Furthermore, the PdO clusters are also highly efficient heterogeneous catalysts for Suzuki coupling reactions [35]. In this work, the PdO layer present on the surface of the catalyst exhibits high reactivity. This is attributed to the strong bonding interaction between the surface atoms of the catalyst and the substrate molecules [36]. The Pd@PdO core–shell structure also enhances the catalytic stability. In fact, the experiments show that the Pd@PdO–NDG catalytic performance is still high after five cycles of Suzuki coupling reaction. To further confirm the structure and morphology change of Pd@PdO–NDG catalyst during the Suzuki reactions, samples after Suzuki coupling reactions were imaged by HRTEM (Fig. S4 in the ESM). The results show a large number of highly uniform Pd@PdO clusters on the NDG, similar to the earlier TEM image. No significant changes could be found, indicating that the substrate material interacts strongly with the Pd clusters. Meanwhile, the XRD patterns of Pd@PdO–NDG after Suzuki coupling reactions also show that the structure and the oxidation state of catalyst have hardly changed0 (Fig. S2 in the ESM). Additionally, the Pd(II) peaks

Table 1 Suzuki coupling reactions with the catalyst Pd@PdO–NDG

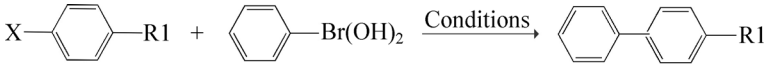

Entry	R1	X	Reaction time (min)	1st cycle yield[a] (%)	2nd cycle yield[a] (%)	3rd cycle yield[a] (%)	4th cycle yield[a] (%)	5th cycle yield[a] (%)
No. 1	$-NO_2$	–Br	60	96	94	93	93	92
No. 2	–CN	–Br	60	95	94	90	89	85
No. 3	$-OCH_3$	–Br	60	90	86	84	82	80

[a] Experimental conditions: phenylboronic acid (0.75 mmol), K_2CO_3 (1.25 mmol), different substrates (0.5 mmol), ethanol solution of Pd@PdO–NDG catalyst (4 mL, 5 mg·mL^{-1}), ethanol (4 mL), 80 ˚C, 60 min. The yield was determined by HPLC and ^{1}H NMR.

and the Pd(0) peaks in XPS spectra for the catalysts before and after Suzuki reaction confirmed the structural stability of the Pd@PdO core–shell (Fig. S5 in the ESM). The peak intensities of Pd(II) and Pd(0) are essentially identical before and after Suzuki reaction, showing there is no change in oxidation state in the Pd@PdO catalysts. Meanwhile, the Pd@PdO–NDG catalyst can be re-used in the Suzuki reaction without any significant loss in catalytic activity and selectivity. The above results show that the stable PdO@Pd core–shell structures on NDG display high activity. The electron-withdrawing nature of the nitrogen atom improves the strength of Pd@PdO and carbon interactions and help to prevent loss of Pd catalyst from the substrate material.

4 Conclusions

The introduction of N-doped graphene can modify nucleation and growth kinetics during Pd@PdO catalyst deposition, which results in smaller Pd@PdO particles, uniform dispersion, and enhanced catalyst durability. Furthermore, the Pd@PdO–NDG catalysts exhibit high yields and good structural stability in C–C cross coupling reactions. N-doped graphene therefore offers new opportunities for heterogeneous catalysis with different metal clusters.

Acknowledgements

This work was supported by the Key Program Projects of the National Natural Science Foundation of China (No. 21031001), the National Natural Science Foundation of China (Nos. 91122018, 21371053, and 51372071), the Cultivation Fund of the Key Scientific and Technical Innovation Project, Ministry of Education of China (No. 708029), the Special Research Fund for the Doctoral Program of Higher Education of China (No. 20112301110002), the Cultivation Fund of Industrialization for Scientific and Technological Achievements of Heilongjiang Province (No. 1253CGZH13), and the Application Technology Research and Development Project of Harbin City (No. 2013AA7BG025). The authors thank beamline BL14W1 (Shanghai Synchrotron Radiation Facility) for providing the beam time.

Electronic Supplementary Material: Supplementary material (TEM images, XRD pattern, and TG-DSC of products; the adsorption energy calculation for the composites and the ^{1}H NMR spectroscopic analysis of the Suzuki reaction products) is available in the online version of this article at http://dx.doi.org/10.1007/s12274-014-0492-1.

References

[1] Miyaura, N.; Suzuki, A. Palladium-catalyzed cross-coupling reactions of organoboron compounds. *Chem. Rev.* **1995**, *95*, 2457–2483.

[2] Hoshiya, N.; Shimoda, M.; Yioshikawa, H.; Yamashita, Y.; Shuto, S.; Arisawa, M. Sulfur modification of Au via treatment with piranha solution provides low-Pd releasing and recyclable Pd material, SAPd. *J. Am. Chem. Soc*. **2010**, *132*, 7270–7272.

[3] Kambe, N.; Iwasaki, T.; Terao, J. Pd-catalyzed cross-coupling reactions of alkyl halides. *Chem. Soc. Rev*. **2011**, *40*, 4937–4947.

[4] Li, Y.; Fan, X. W.; Liu, Z. F.; Liu, Z. R. Strain effects in graphene and graphene nanoribbons: The underlying mechanism. *Nano Res*. **2010**, *3*, 545–556.

[5] Tian, N.; Zhou, Z. Y.; Sun, S. G.; Ding, Y.; Wang, Z. L. Synthesis of tetrahexahedral platinum nanocrystals with high index facets and high electrooxidation activity. *Science* **2007**, *316*, 732–735.

[6] Yang, J.; Tian, C. G.; Wang, L.; Fu, H. G. An effective strategy for small-sized and highly-dispersed palladium nanoparticles supported on graphene with excellent performance for formic acid oxidation. *J. Mater. Chem.* **2011**, *21*, 3384–3390.

[7] Zlotea, C.; Cuevas, F.; Paul-Boncour, V.; Leroy, E.; Dibandjo, P.; Gadiou, R.; Vix-Guterl, C.; Latroche, M. Size-dependent hydrogen sorption in ultrasmall Pd clusters embedded in a mesoporous carbon template. *J. Am. Chem. Soc.* **2010**, *132*, 7720–7729.

[8] Mitsudome, T.; Nose, K.; Mori, K.; Mizugaki, T.; Ebitani, K.; Jitsukawa, K.; Kaneda, K. Montmorillonite-entrapped sub-nanoordered Pd clusters as a heterogeneous catalyst for allylic substitution reactions. *Angew. Chem. Int. Ed.* **2007**, *46*, 3288–3290.

[9] Amoroso, F.; Colussi, S.; Zotto, A. D.; Llorca, J.; Trovarelli, A. PdO hydrate as an efficient and recyclable catalyst for the Suzuki–Miyaura reaction in water/ethanol at room temperature. *Catal. Commun*. **2011**, *12*, 563–567.

[10] White, R. J.; Luque, R.; Budarin, V. L.; Clark, J. H.; MacQuarrie, D. J. Supported metal nanoparticles on porous materials. Methods and applications. *Chem. Soc. Rev.* **2009**, *38*, 481–494.

[11] Xiong, Y. J.; Chen, J. Y.; Wiley, B.; Xia, Y. N.; Yin, Y. D.; Li, Z. Y. Size-dependence of surface plasmon resonance and oxidation for Pd nanocubes synthesized via a seed etching process. *Nano Lett.* **2005**, *7*, 1237–1242.

[12] Pylypenko, S.; Queen, A.; Olson, T. S.; Dameron, A.; O'Neill, K.; Neyerlin, K. C.; Pivovar, B.; Dinh, H. N.; Ginley, D. S.; Gennett, T. et al. Tuning carbon-based fuel cell catalyst support structures via nitrogen functionalization. I. Investigation of structural and compositional modification of highly oriented pyrolytic graphite model catalyst supports as a function of nitrogen implantation dose. *J. Phys. Chem. C* **2011**, *115*, 13667–13675.

[13] Pylypenko, S.; Borisevich, A.; More, K. L.; Corpuz, A. R.; Holme, T.; Dameron, A. A.; Olson, T. S.; Dinh, H. N.; Gennette, T.; O'Hayre, R. Nitrogen: Unraveling the secret to stable carbon-supported Pt-alloy electrocatalysts. *Energy Environ. Sci.* **2013**, *6*, 2957–2964.

[14] Novoselov, K. S.; Geim, A. K.; Morozov, S. V.; Jiang, D.; Zhang, Y.; Dubonos, S. V.; Grigorieva, I. V.; Firsov, A. A. Electric field effect in atomically thin carbon films. *Science* **2004**, *306*, 666–669.

[15] Jiang, B. J.; Tian, C. G.; Zhou, W.; Wang, J. Q.; Xie, Y.; Pan, Q. J.; Ren, Z. Y.; Dong, Y. Z.; Fu, D.; Han, J. L. et al. *In situ* growth of TiO_2 in interlayers of expanded graphite for the fabrication of TiO_2–graphene with enhanced photocatalytic activity. *Chem.–Eur. J.* **2011**, *17*, 8379–8387.

[16] Jiang, B. J.; Tian, C. G.; Pan, Q. J.; Jiang, Z.; Wang, J. Q.; Yan, W. S.; Fu, H. G. Enhanced photocatalytic activity and electron transfer mechanisms of graphene/TiO_2 with exposed {001} facets. *J. Phys. Chem. C* **2011**, *115*, 23718–23725.

[17] Jiang, B. J.; Tian, C. G.; Wang, L.; Xu, Y. X.; Wang, R. H.; Qiao, Y. J.; Ma, Y. G.; Fu, H. G. Facile fabrication of high quality graphene from expandable graphite: Simultaneous exfoliation and reduction. *Chem. Commun.* **2010**, *46*, 4920–4922.

[18] Jiang, B. J.; Wang, Y. H.; Wang, J. Q.; Tian, C. G.; Li, W. J.; Feng, Q. M.; Pan, Q. J.; Fu, H. G. *In situ* fabrication of Ag/Ag_3PO_4/graphene triple heterostructure visible light photocatalyst via graphene-assisted reduction strategy. *ChemCatChem* **2013**, *5*, 1359–1367.

[19] Scheuermann, G. M.; Rumi, L.; Steurer, P.; Bannwarth, W.; Mülhaupt, R. Palladium nanoparticles on graphite oxide and its functionalized graphene derivatives as highly active catalysts for the Suzuki–Miyaura coupling reaction. *J. Am. Chem. Soc.* **2009**, *131*, 8262–8270.

[20] Li, X. L.; Wang, H. L.; Robinson, J. T.; Sanchez, H.; Diankov, G.; Dai, H. J. Simultaneous nitrogen doping and reduction of graphene oxide. *J. Am. Chem. Soc.* **2009**, *131*, 15939–15944.

[21] Sun, X. M.; Luo, D. C.; Liu, J. F.; Evans, D. G. Monodisperse chemically modified graphene obtained by density gradient ultracentrifugal rate separation. *ACS Nano* **2010**, *4*, 3381–3389.

[22] Jiang, B. J.; Tian, C. G.; Wang, L.; Sun, L.; Chen, C.; Nong, X. Z.; Qiao, Y. J.; Fu, H. G. Highly concentrated, stable nitrogen-doped graphene for supercapacitors: Simultaneous doping and reduction. *Appl. Surf. Sci*. **2012**, *258*, 3438–3443.

[23] Bradley, J. S. Millar; J. M. Hill, E. W. Surface chemistry on colloidal metals: A high-resolution NMR study of carbon monoxide adsorbed on metallic palladium crystallites in colloidal suspension. *J. Am. Chem. Soc.* **1991**, *113*, 4016–4017.

[24] López-Corral, I.; Germán, E.; Juan, A.; Volpe, M. A.; Brizuela, G. P. DFT study of hydrogen adsorption on palladium decorated graphene. *J. Phys. Chem. C* **2011**, *115*, 4315–4323.

[25] Chen, X. M.; Wu, G. H.; Chen, J. M.; Chen, X.; Xie, Z. X.; Wang, X. R. Synthesis of "clean" and well-dispersive Pd nanoparticles with excellent electrocatalytic property on graphene oxide. *J. Am. Chem. Soc.* **2011**, *133*, 3693–3695.

[26] Hu, Z. L.; Aizawa, M.; Wang, Z. M.; Yoshizawa, N.; Hatori, H. Synthesis and characteristics of graphene oxide-derived carbon nanosheet–Pd nanosized particle composites. *Langmuir* **2010**, *26*, 6681–6688.

[27] Moussa, S.; Siamaki, A. R.; Gupton, B. F.; El-Shall, M. S. Pd-partially reduced graphene oxide catalysts (Pd/PRGO): Laser synthesis of Pd nanoparticles supported on PRGO nanosheets for carbon-carbon cross coupling reactions. *ACS Catal.* **2012**, *2*, 145–154.

[28] Zhang, H. B.; Pan, X. L.; Liu, J. Y.; Qian, W. Z.; Wei, F.; Huang, Y. Y.; Bao, X. H. Enhanced catalytic activity of sub-nanometer titania clusters confined inside double-wall carbon nanotubes. *ChemSusChem* **2011**, *4*, 975–980.

[29] Sheng, Z. H.; Shao, L.; Chen, J. J.; Bao, W. J.; Wang, F. B.; Xia, X. H. Catalyst-free synthesis of nitrogen-doped graphene via thermal annealing graphite oxide with melamine and its excellent electrocatalysis. *ACS Nano* **2011**, *28*, 4350–4358.

[30] Soriano, L.; Fuentes, G. G.; Quirós, C.; Trigo, J. F.; Sanz, J. M.; Bressler, P. R.; González-Elipe, A. R. Crystal-field effects at the TiO_2–SiO_2 interface as observed by X-ray absorption spectroscopy. *Langmuir* **2000**, *16*, 7066–7069.

[31] Chen, C. H.; Hwang, B. J.; Wang, G. R.; Sarma, L. S.; Tang, M. T.; Liu, D. G.; Lee, J. F. Nucleation and growth mechanism of Pd/Pt bimetallic clusters in sodium bis(2-ethylhexyl)sulfosuccinate (AOT) reverse micelles as

studied by *in situ* X-ray absorption spectroscopy. *J. Phys. Chem. B* **2005**, *109*, 21566–21575.

[32] Moussa, S.; Siamaki, A. R.; Gupton, B. F.; El-Shall, M. S. Pd-partially reduced graphene oxide catalysts (Pd/PRGO): Laser synthesis of Pd nanoparticles supported on PRGO nanosheets for carbon–carbon cross coupling reactions. *ACS Catal.* **2012**, *2*, 145–154.

[33] Zhou, Y. K.; Pasquarelli, R.; Holme, T.; Berry, J.; Ginley, D.; O'Hayre, R. Improving PEM fuel cell catalyst activity and durability using nitrogen-doped carbon supports: Observations from model Pt/HOPG systems. *J. Mater. Chem.* **2009**, *19*, 7830–7838.

[34] Deraedt, C.; Astruc, D. "Homeopathic" palladium nanoparticle catalysis of cross carbon-carbon coupling reactions. *Acc. Chem. Res.* **2014**, *47*, 494–503.

[35] Ohtaka, A.; Teratani, T.; Fujii, R.; Ikeshita, K.; Kawashima, T.; Tatsumi, K.; Shimomura, O.; Nomura, R. Linear polystyrene-stabilized palladium nanoparticles-catalyzed C–C coupling reaction in water. *J. Org. Chem.* **2011**, *76*, 4052–4060.

[36] Su, H. L.; Dong, Q.; Han, J.; Zhang, D.; Guo, Q. X. Biogenic synthesis and photocatalysis of Pd–PdO nanoclusters reinforced hierarchical TiO_2 films with interwoven and tubular conformations. *Biomacromolecules* **2008**, *9*, 499–504.